How to Kill a Penguin

Ulrich Haisch

Universität Zürich - Institut für Theoretische Physik
CH-8057 Zürich - Switzerland

Within constrained minimal-flavor-violation the large destructive flavor-changing Z-penguin managed to survive eradication so far. We give a incisive description of how to kill it using the precision measurements of the $Z \to b\bar{b}$ pseudo observables. The derived stringent range for the non-standard contribution to the universal Inami-Lim function C leads to tight two-sided limits for the branching ratios of all Z-penguin dominated flavor-changing K- and B-decays.

1 Introduction

The effects of new heavy particles appearing in extensions of the standard model (SM) can be accounted for at low energies in terms of effective operators. The unprecedented accuracy reached by the electroweak (EW) precision measurements performed at the high-energy colliders LEP and SLC impose stringent constraints on the coefficients of the operators entering the EW sector. Other severe constraints came in recent years from the BaBar, Belle, CDF, and DØ experiments and concern extra sources of flavor and *CP* violation that represent a generic problem in many scenarios of new physics (NP). The most pessimistic but experimentally well supported solution to the flavor puzzle is to assume that all flavor and *CP* violation is governed by the known structure of the SM Yukawa interactions. In these minimal-flavor-violating (MFV) [2, 3, 4] models correlations between certain flavor diagonal high-energy and flavor off-diagonal low-energy observables exist since, by construction, NP couples dominantly to the third generation. In order to simplify matters, we restrict ourselves in the following to the class of constrained MFV (CMFV) [5] models, i.e., scenarios that involve only SM operators, and thus consider just left-handed currents.

2 General considerations

That new interactions unique to the third generation can lead to an intimate relation between the non-universal $Zb_L\bar{b}_L$ and the flavor non-diagonal $Zd_L^j\bar{d}_L^i$ vertices has been shown recently in [6]. Whereas the former structure is probed by the ratio of the Z-boson decay width into bottom quarks and the total hadronic width, R_b^0, the bottom quark asymmetry parameter, $\mathcal{A}_b$, and the forward-backward asymmetry for bottom quarks, $A_{\rm FB}^{0,b}$, the latter ones appear in many K- and B-decays.

In the effective field theory framework of MFV [4], one can easily see how the $Zb_L\bar{b}_L$ and $Zd_L^j\bar{d}_L^i$ operators are linked together. The only relevant dimension-six contributions compatible with the flavor group of MFV stem from the $SU(2) \times U(1)$ invariant operators

$$\begin{aligned} \mathcal{O}_1 &= i\left(\bar{Q}_L Y_U Y_U^\dagger \gamma_\mu Q_L\right) \phi^\dagger D^\mu \phi\,, \\ \mathcal{O}_2 &= i\left(\bar{Q}_L Y_U Y_U^\dagger \tau^a \gamma_\mu Q_L\right) \phi^\dagger \tau^a D^\mu \phi\,, \end{aligned} \tag{1}$$

that are built out of the quark doublets Q_L, the Higgs field ϕ, the up-type Yukawa matrices Y_U, and the $SU(2)$ generators τ^a. After EW symmetry breaking, $\mathcal{O}_{1,2}$ are responsible for

both the effective $Zb_L\bar{b}_L$ and $Zd_L^j\bar{d}_L^i$ vertex. Since all up-type quark Yukawa couplings except the one of the top, y_t, are small, one has $(Y_U Y_U^\dagger)_{ji} \sim y_t^2 V_{tj}^* V_{ti}$ and only this contribution matters in Eq. (1).

Within the SM the Feynman diagrams responsible for the enhanced top correction to the $Zb_L\bar{b}_L$ coupling also generate the $Zd_L^j\bar{d}_L^i$ operators. In fact, in the limit of infinite top quark mass the corresponding amplitudes are up to Cabibbo-Kobayashi-Maskawa (CKM) factors identical. Yet there is a important difference between them. While for the physical $Z \to b\bar{b}$ decay the diagrams are evaluated on-shell, in the case of the low-energy $Z \to d^j\bar{d}^i$ transitions the amplitudes are Taylor-expanded up to zeroth order in the external momenta. As far as the momentum of the Z-boson is concerned the two cases correspond to $q^2 = M_Z^2$ and $q^2 = 0$.

The general features of the small momentum expansion of the one-loop $Z \to b\bar{b}$ vertex can be nicely illustrated with the following simple but educated example. Consider the scalar integral

$$C_0 = \frac{m_3^2}{i\pi^2} \int \frac{d^4l}{D_1 D_2 D_3}\,, \qquad (2)$$

with $D_i = (l + p_i)^2 - m_i^2$ and $p_3 = 0$. Note that we have set the space-time dimension to four since the integral is finite and assumed without loss of generality $m_3 \neq 0$.

In the limit of vanishing bottom quark mass one has for the corresponding momenta $p_1^2 = p_2^2 = 0$. The small momentum expansion of the scalar integral C_0 then takes the form

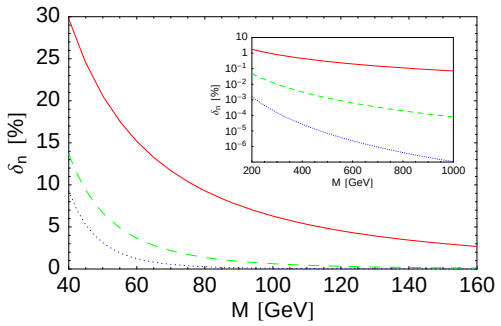

Figure 1: Relative deviations δ_n as a function of M. The solid, dashed, and dotted curve correspond to $n = 1, 2$, and 3, respectively. See text for details.

$$C_0 = \sum_{n=0}^{\infty} a_n \left(\frac{q^2}{m_3^2}\right)^n\,, \qquad (3)$$

with $q^2 = (p_1 - p_2)^2 = -2p_1 \cdot p_2$. The expansion coefficients a_n are given by [7]

$$a_n = \frac{(-1)^n}{(n+1)!} \sum_{l=0}^{n} \binom{n}{l} \frac{x_1^l}{l!} \frac{\partial^l}{\partial x_1^l} \frac{\partial^n}{\partial x_2^n} g(x_1, x_2)\,, \qquad (4)$$

where

$$g(x_1, x_2) = \frac{1}{x_1 - x_2} \left(\frac{x_1 \ln x_1}{1 - x_1} - \frac{x_2 \ln x_2}{1 - x_2}\right)\,, \qquad (5)$$

and $x_i = m_i^2/m_3^2$. Notice that in order to properly generate the expansion coefficients a_n one has to keep x_1 and x_2 different even in the zero or equal mass case. The corresponding limits can only be taken at the end.

To illustrate the convergence behavior of the small momentum expansion of the scalar integral in Eq. (3) for on-shell kinematics, we confine ourselves to the simplified case $m_1 = m_2 = M$ and $m_3 = m_t$. We define

$$\delta_n = a_n \left(\frac{M_Z^2}{m_t^2}\right)^n \left(\sum_{l=0}^{n-1} a_l \left(\frac{M_Z^2}{m_t^2}\right)^l\right)^{-1}\,, \qquad (6)$$

for $n = 1, 2, \ldots$. The M-dependence of the relative deviations δ_n is displayed in Fig. 1. We see that while for $M \lesssim 50\,\text{GeV}$ higher order terms in the small momentum expansion have to be included in order to approximate the exact on-shell result accurately, in the case of $M \gtrsim 150\,\text{GeV}$ the first correction is small and higher order terms are negligible. For the two reference scales $M = \{80, 250\}\,\text{GeV}$ one finds for the first three relative deviations δ_n numerically +9.3%, +1.4%, and +0.3%, and +1.1%, +0.02%, +0.00004%, respectively.

3 Model calculations

The above considerations can be corroborated in another, yet model-dependent way by calculating explicitly the difference between the value of the $Zd^j_L\bar{d}^i_L$ vertex form factor evaluated on-shell and at zero external momenta. In [6] this has been done in four of the most popular, consistent, and phenomenologically viable scenarios of CMFV, i.e., the two-Higgs-doublet model (THDM) type I and II, the minimal-supersymmetric SM (MSSM) with MFV [3], all for small $\tan\beta$, the minimal universal extra dimension (mUED) model [8], and the littlest Higgs model [9] with T-parity (LHT) [10] and degenerate mirror fermions [11]. In the following we will briefly summarize the most important findings of [6].

In the limit of vanishing bottom quark mass, possible non-universal NP contributions to the renormalized off-shell $Zd^j_L\bar{d}^i_L$ vertex can be written as

$$\Gamma^{\text{NP}}_{ji} = \frac{G_F}{\sqrt{2}}\frac{e}{\pi^2}M_z^2\frac{c_W}{s_W}V^*_{tj}V_{ti}C_{\text{NP}}(q^2)\bar{d}^j{}_L\gamma_\mu d^i{}_L Z^\mu\,, \tag{7}$$

where $i = j = b$ and $i \neq j$ in the flavor diagonal and off-diagonal case. G_F, e, s_W, and c_W denote the Fermi constant, the electromagnetic coupling constant, the sine and cosine of the weak mixing angle, respectively, while V_{ij} are the corresponding CKM matrix elements.

As a measure of the relative difference between the complex valued form factor $C_{\text{NP}}(q^2)$ evaluated on-shell and at zero momentum we introduce

$$\delta C_{\text{NP}} = 1 - \frac{\text{Re}\,C_{\text{NP}}(q^2 = 0)}{\text{Re}\,C_{\text{NP}}(q^2 = M_z^2)}\,. \tag{8}$$

The dependence of δC_{NP} on the charged Higgs mass $M_H^\pm$, the lighter chargino mass $M_{\tilde{\chi}_1}^\pm$, the compactification scale $1/R$, and x_L which parameterizes the mass of the heavy top T_+ is illustrated in Fig. 2. The allowed parameter regions after applying experimental and theoretical constraints are indicated by the colored (grayish) bands and points.

In the THDMs, the mUED, and the CMFV version of the LHT model the maximal allowed suppressions of $\text{Re}\,C_{\text{NP}}(q^2 = M_z^2)$ with respect to $\text{Re}\,C_{\text{NP}}(q^2 = 0)$ amounts to less than 2%, 5%, and 4%, respectively. This feature confirms the general argument presented in the last section. The situation is less favorable in the case of the CMFV MSSM, since δC_{MSSM} frequently turns out to be larger than one would expected on the basis of the model-independent considerations if the masses of the lighter chargino and stop both lie in the hundred GeV range. However, the large deviation δC_{MSSM} are ultimately no cause of concern, because $|\text{Re}\,C_{\text{MSSM}}(q^2 = 0)/\text{Re}\,C_{\text{SM}}(q^2 = 0)|$ itself is always below 10%. In consequence, the model-independent bounds on the NP contribution to the universal Z-penguin function that will be derived in the next section do hold in the case of the CMFV MSSM. More details on the phenomenological analysis of δC_{NP} in the THDMs, the CMFV MSSM, the mUED, and the LHT model including the analytic expressions for the form factors $C_{\text{NP}}(q^2)$ can be found in the recent article [6].

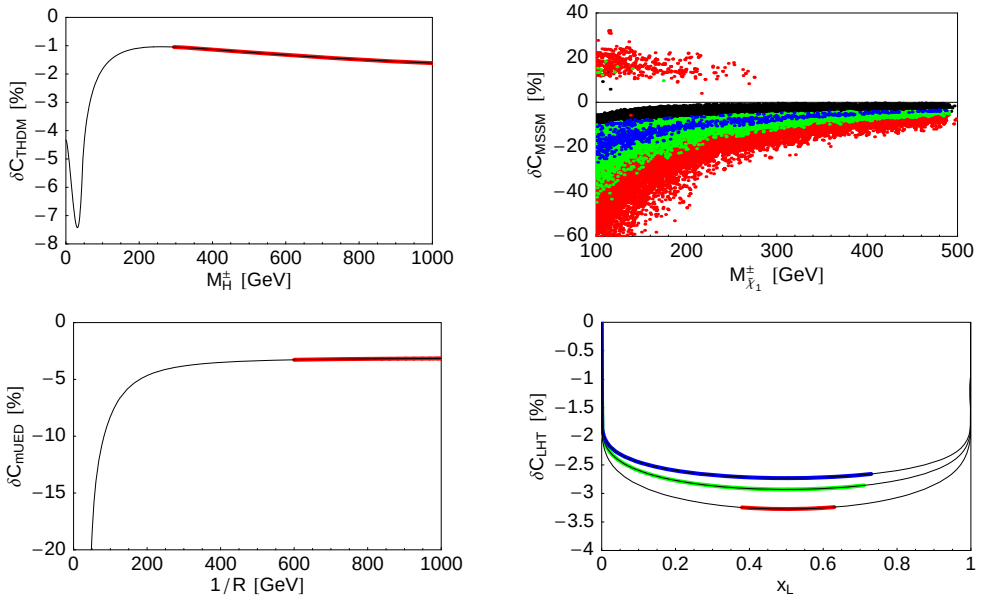

Figure 2: Relative difference $\delta C_{\rm NP}$ in the THDMs, the MSSM, the mUED, and the LHT model as a function of $M_H^\pm$, $M_{\tilde\chi_1}^\pm$, $1/R$, and x_L. Regions in the $M_{\tilde\chi_1}^\pm - \delta C_{\rm MSSM}$ plane where $|\mathrm{Re}\, C_{\rm MSSM}(q^2=0)|$ amounts to at least 2%, 4%, and 6% of $|\mathrm{Re}\, C_{\rm SM}(q^2=0)|$ are indicated by the red (gray), green (light gray), and blue (dark gray) points, respectively. In the case of the LHT model the shown curves correspond, from bottom to top, to the values $f = 1, 1.5$, and 2 TeV of the symmetry breaking scale. See text for details.

4 Numerical analysis

Using the technique of epsilon parameters a model-independent numerical analysis of $\Delta C = \mathrm{Re}\, C(q^2=0) - \mathrm{Re}\, C_{\rm SM}(q^2=0)$ is a back-on-the-envelope calculation. The variation $\epsilon_b^{\rm NP} = \epsilon_b - \epsilon_b^{\rm SM}$ arising from NP contributions to $Zb_L\bar b_L$ can be defined through the inclusive partial width of $Z \to b\bar b$ as follows [12]

$$\Gamma_{bb}^{\rm NP} = (\sqrt{2} G_F M_Z^2)^{\frac{1}{2}} \left(g_V^b (\bar b \gamma_\mu b) - g_A^b (\bar b \gamma_\mu \gamma_5 b) \right) Z^\mu \,, \tag{9}$$

where

$$\frac{g_V^b}{g_A^b} = \left(1 + \frac{4 s_W^2}{3} + \epsilon_b^{\rm NP} \right) \frac{g_A^d}{g_A^b} \,, \quad g_A^b = (1 + \epsilon_b^{\rm NP})\, g_A^d \,. \tag{10}$$

From Eqs. (7), (8), and (9) one obtains

$$\Delta C = - \frac{\pi^2}{\sqrt{2} G_F M_Z^2 c_W^2} (1 + \delta C_{\rm NP})\, \epsilon_b^{\rm NP} \,. \tag{11}$$

By combining experimental [13] and theoretical uncertainties [15] in ϵ_b and $\epsilon_b^{\rm SM}$ linearly one finds

$$\epsilon_b^{\rm NP} = (0.4 \pm 2.5) \times 10^{-3}\,. \qquad (12)$$

Assuming $\delta C_{\rm NP} = \pm 0.1$ one then arrives at

$$\Delta C = -0.04 \pm 0.26\,, \qquad (13)$$

which implies that large negative contributions that would reverse the sign of the SM Z-penguin amplitude are highly disfavored in CMFV scenarios due to the strong constraint from R_b^0 [6]. Interestingly, such a conclusion cannot be drawn by considering only flavor constraints [14], since a combination of $\mathcal{B}(\bar B \to X_s\gamma)$, $\mathcal{B}(\bar B \to X_s l^+ l^-)$, and $\mathcal{B}(K^+ \to \pi^+ \nu\bar\nu)$ does not allow to distinguish the SM solution $\Delta C = 0$ from the wrong-sign case $\Delta C \approx -2$ at present.

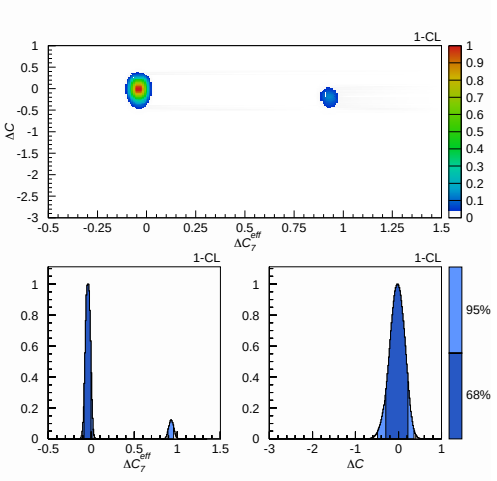

Figure 3: Constraints on $\Delta C_7^{\rm eff}$ and ΔC within CMFV that follow from a combination of the $Z \to b\bar b$ POs with the measurements of $\bar B \to X_s\gamma$ and $\bar B \to X_s l^+ l^-$. The colors encode the frequentist $1-{\rm CL}$ level and the corresponding 68% and 95% probability regions as indicated by the bars on the right side of the panels. See text for details.

The result in Eq. (13) agrees amazingly well with the numbers of a thorough global fit to the POs R_b^0, $\mathcal{A}_b$, and $A_{\rm FB}^{0,b}$ [13] and the measured $\bar B \to X_s\gamma$ [17] and $\bar B \to X_s l^+ l^-$ [18] BRs obtained by employing customized versions of the `ZFITTER` [15] and the CKMfitter package [19]. Neglecting contributions from EW boxes these bounds read [6]

$$\begin{aligned} \Delta C &= -0.026 \pm 0.264 \quad (68\%\,{\rm CL})\,, \\ \Delta C &= [-0.483, 0.368] \quad (95\%\,{\rm CL})\,. \end{aligned} \qquad (14)$$

The constraint on ΔC within CMFV following from the simultaneous use of R_b^0, $\mathcal{A}_b$, $A_{\rm FB}^{0,b}$, $\mathcal{B}(\bar B \to X_s\gamma)$, and $\mathcal{B}(\bar B \to X_s l^+ l^-)$ can be seen in Fig. 3.

One can also infer from this figure that two regions, resembling the two possible signs of the amplitude $\mathcal{A}(b \to s\gamma) \propto C_7^{\rm eff}(m_b)$, satisfy all existing experimental bounds. The best fit value for $\Delta C_7^{\rm eff} = C_7^{\rm eff}(m_b) - C_{7\,{\rm SM}}^{\rm eff}(m_b)$ is very close to the SM point residing in the origin, while the wrong-sign solution located on the right is highly disfavored, as it corresponds to a $\mathcal{B}(\bar B \to X_s l^+ l^-)$ value considerably higher than the measurements [20]. The corresponding limits are [6]

$$\begin{aligned} \Delta C_7^{\rm eff} &= -0.039 \pm 0.043 \quad (68\%\,{\rm CL})\,, \\ \Delta C_7^{\rm eff} &= [-0.104, 0.026] \cup [0.890, 0.968] \quad (95\%\,{\rm CL})\,. \end{aligned} \qquad (15)$$

Similar bounds have been presented previously in [14]. Notice that since the SM prediction of $\mathcal{B}(\bar B \to X_s\gamma)$ [16] is now lower than the experimental world average by $1.2\,\sigma$, extensions of the SM that predict a suppression of the $b \to s\gamma$ amplitude are strongly constrained. In particular, even the SM point $\Delta C_7^{\rm eff} = 0$ is almost disfavored at 68% CL by the global fit.

The stringent bound on the NP contribution ΔC given in Eq. (14) translates into tight two-sided limits for the BRs of all Z-penguin dominated flavor-changing K- and B-decays as

Observable	CMFV	SM	Experiment
$\mathcal{B}(K^+ \to \pi^+ \nu\bar{\nu}) \times 10^{11}$	$[4.29, 10.72]$	$[5.40, 9.11]$	$\left(14.7^{+13.0}_{-8.9}\right)$ [21]
$\mathcal{B}(K_L \to \pi^0 \nu\bar{\nu}) \times 10^{11}$	$[1.55, 4.38]$	$[2.21, 3.45]$	$< 2.1 \times 10^4$ (90% CL) [22]
$\mathcal{B}(K_L \to \mu^+\mu^-)_{\rm SD} \times 10^9$	$[0.30, 1.22]$	$[0.54, 0.88]$	–
$\mathcal{B}(\bar{B} \to X_d \nu\bar{\nu}) \times 10^6$	$[0.77, 2.00]$	$[1.24, 1.45]$	–
$\mathcal{B}(\bar{B} \to X_s \nu\bar{\nu}) \times 10^5$	$[1.88, 4.86]$	$[3.06, 3.48]$	< 64 (90% CL) [23]
$\mathcal{B}(B_d \to \mu^+\mu^-) \times 10^{10}$	$[0.36, 2.03]$	$[0.87, 1.27]$	$< 3.0 \times 10^2$ (95% CL) [24]
$\mathcal{B}(B_s \to \mu^+\mu^-) \times 10^9$	$[1.17, 6.67]$	$[2.92, 4.13]$	$< 9.3 \times 10^1$ (95% CL) [25]

Table 1: Bounds for various rare decays in CMFV and the SM at 95% CL. The available experimental information is also shown. See text for details.

shown in Tab. 4. A strong violation of any of the bounds by future measurements will imply a failure of the CMFV assumption, signaling either the presence of new effective operators and/or new flavor and CP violation. A way to evade the given limits is the presence of sizable corrections $\delta C_{\rm NP}$ and/or box contributions. While these possibilities cannot be fully excluded, general arguments and explicit calculations indicate that they are both difficult to realize in the CMFV framework.

5 Conclusions

R.I.P. large destructive CMFV Z-penguin!

6 Post scriptum

Assuming the correctness of the SM, the $1.2\,\sigma$ deviation between the most recent SM prediction [16] and the measured value of $\bar{B} \to X_s\gamma$ can be accommodated by a value of the strong coupling constant that is higher than the world average of $\alpha_s(M_Z)$ [26]. Using the same input as in [16], the next-to-next-to-leading order SM estimate and the measurements of $\bar{B} \to X_s\gamma$ would agree within errors for the nominal value

$$\alpha_s(M_Z) = 0.129 \pm 0.006_{\rm expt} \pm 0.005_{\rm theo}\,. \tag{16}$$

Of course, trying to explain the slight tension in $\bar{B} \to X_s\gamma$ by a shift in $\alpha_s(M_Z)$ should be considered a purely academic exercise. Nothing more, nothing less.

Acknowledgments

I am grateful to A. Weiler for fruitful collaboration, valuable comments on the manuscript, and technical support. A big thank you to A. Banfi for encouraging me to extract a value for $\alpha_s(M_Z)$ from $\bar{B} \to X_s\gamma$. This work has been supported by the Schweizer Nationalfonds.

References

[1] Slides:
`http://indico.cern.ch/contributionDisplay.py?contribId=117&sessionId=9&confId=9499`

[2] R. S. Chivukula and H. Georgi, Phys. Lett. B **188**, 99 (1987).

[3] E. Gabrielli and G. F. Giudice, Nucl. Phys. B **433**, 3 (1995) [Erratum-ibid. B **507**, 549 (1997)]; A. Ali and D. London, Eur. Phys. J. C **9**, 687 (1999); A. J. Buras *et al.*, Phys. Lett. B **500**, 161 (2001).

[4] G. D'Ambrosio *et al.*, Nucl. Phys. B **645**, 155 (2002).

[5] M. Blanke *et al.*, JHEP **0610**, 003 (2006) and references therein.

[6] U. Haisch and A. Weiler, 0706.2054 [hep-ph].

[7] J. Fleischer and O. V. Tarasov, Z. Phys. C **64**, 413 (1994).

[8] T. Appelquist, H. C. Cheng and B. A. Dobrescu, Phys. Rev. D **64**, 035002 (2001).

[9] N. Arkani-Hamed *et al.*, JHEP **0207**, 034 (2002).

[10] H. C. Cheng and I. Low, JHEP **0309**, 051 (2003) and **0408**, 061 (2004).

[11] I. Low, JHEP **0410**, 067 (2004).

[12] G. Altarelli, R. Barbieri and F. Caravaglios, Nucl. Phys. B **405**, 3 (1993) and Phys. Lett. B **314**, 357 (1993).

[13] S. Schael *et al.*, Phys. Rept. **427**, 257 (2006).

[14] C. Bobeth *et al.*, Nucl. Phys. B **726**, 252 (2005).

[15] D. Y. Bardin *et al.*, Comput. Phys. Commun. **133**, 229 (2001); A. B. Arbuzov *et al.*, Comput. Phys. Commun. **174**, 728 (2006) and `http://www-zeuthen.desy.de/theory/research/zfitter/index.html`

[16] M. Misiak *et al.*, Phys. Rev. Lett. **98**, 022002 (2007); M. Misiak and M. Steinhauser, Nucl. Phys. B **764**, 62 (2007).

[17] S. Chen *et al.* [CLEO Collaboration], Phys. Rev. Lett. **87**, 251807 (2001); P. Koppenburg *et al.* [Belle Collaboration], Phys. Rev. Lett. **93**, 061803 (2004); B. Aubert *et al.* [BaBar Collaboration], Phys. Rev. Lett. **97**, 171803 (2006).

[18] B. Aubert *et al.* [BaBar Collaboration], Phys. Rev. Lett. **93**, 081802 (2004); K. Abe *et al.* [Belle Collaboration], hep-ex/0408119.

[19] J. Charles *et al.* [CKMfitter Group], Eur. Phys. J. C **41**, 1 (2005) and `http://ckmfitter.in2p3.fr/`

[20] P. Gambino, U. Haisch and M. Misiak, Phys. Rev. Lett. **94**, 061803 (2005).

[21] S. C. Adler *et al.* [E787 Collaboration], Phys. Rev. Lett. **79**, 2204 (1997), **84**, 3768 (2000), **88**, 041803 (2002) and Phys. Rev. D **70**, 037102 (2004); V. V. Anisimovsky *et al.* [E949 Collaboration], Phys. Rev. Lett. **93**, 031801 (2004).

[22] J. K. Ahn *et al.* [E391a Collaboration], Phys. Rev. D **74**, 051105 (2006) [Erratum-ibid. **74**, 079901 (2006)].

[23] R. Barate *et al.* [ALEPH Collaboration], Eur. Phys. J. C **19**, 213 (2001).

[24] R. P. Bernhard, hep-ex/0605065.

[25] A. Sanchez-Hernandez, talk given at Rencontres de Moriond "Electroweak interactions and Unified theories", La Thuile, Italy, March 10-17, 2007, `http://moriond.in2p3.fr/`

[26] W. M. Yao *et al.* [Particle Data Group], J. Phys. G **33**, 1 (2006); S. Bethke, Prog. Part. Nucl. Phys. **58**, 351 (2007).